Lab on a Chip

Cite this: DOI: 10.1039/c1lc20108e

www.rsc.org/loc

COMMUNICATION

Air-bubble-triggered drop formation in microfluidics†

Adam R. Abate* and David A. Weitz

Received 6th February 2011, Accepted 17th March 2011
DOI: 10.1039/c1lc20108e

In microfluidic devices, droplets are normally formed using T-junction or flow focus mechanisms. While both afford a high degree of control over drop formation, they are limited in maximum production rate by the jetting transition. Here, we introduce a new drop formation mechanism that is not limited by jetting, allowing much faster drop production.

Microfluidic devices can form emulsions with controlled properties, in which all the drops are identical in shape and of a size that can be selected.[1–5] The controlled properties of these emulsions make them attractive for a range of applications. For example, the droplets can be used as templates by which to synthesize particles with a variety of properties, including spherical colloids, non-spherical microgels, and core-shell capsules.[6–10] Alternatively, the drops can be used as tiny "test tubes" within which to perform chemical or biological reactions; due to the uniformity of the drops and their small size, large numbers of reactions can be performed with precision, and using a minimal amount of reagent.[11–15]

Drop formation is normally achieved using either T-junction or flow focus mechanisms.[16–18] While both can form monodisperse drops, they are limited in maximum production rate by the dripping-to-jetting transition.[19,20] At jetting, the system transitions from the periodic formation of monodisperse drops to the formation of long jets that break into polydisperse drops.[21] The polydispersity of emulsions formed at these flow rates limits their attractiveness for most applications; consequently, with microfluidic devices using these mechanisms, drops are almost always formed under slow, controlled flow conditions. For the rate of drop formation to be increased, for faster production of particles or processing of reactions, a new mechanism is needed that can operate under the high flow rates of jetting.

In this paper, we introduce a new drop formation mechanism that can operate under the high flow rates of jetting; consequently, it can form drops much faster than either T-junction or flow focus mechanisms. To form drops, we create a jet of the dispersed fluid in a microfluidic channel by flowing at very high flow rates. In the absence of other forces, the jet is stable and does not break into drops.[17,22,23] However, by forcing air bubbles alongside the jet and confining both in a narrow channel, we create curved regions in the water–oil interface that are unstable to the Rayleigh–Plateau instability. The fluid between consecutive bubbles becomes the drops, so that by adjusting bubble spacing we control drop size, and by using evenly-spaced bubbles, form monodisperse drops. The mechanism can be used to form single and double emulsions.

To form drops with this mechanism, we construct a microfluidic device consisting of three components: a jetting junction for the creation of a stable jet of the dispersed phase, a bubbling junction for formation of monodisperse air bubbles, and a triggering junction, in which the bubbles are squeezed into the jet, to break it into drops. The jetting and bubbling junctions sit upstream in the device, with their outlets intersecting at the triggering junction, as pictured in Fig. 1. The dispersed phase is injected into the inlet of the jetting junction, and air and continuous phase into the T-junction. This creates a jet of the dispersed phase that extends into the triggering junction, while the T-junction forms air bubbles flowed alongside the jet. Even though the flow velocities are very high to enable jetting of the dispersed phase, the air does not jet due to its flow characteristics. For example, due to the low density of air, the inertia of the flow is small even for very high velocities. Additionally, due to the high surface tension of air with liquids, interfacial forces are larger by comparison, enabling faster pinching of the air stream. Combined, these characteristics enable periodic, monodisperse bubble formation

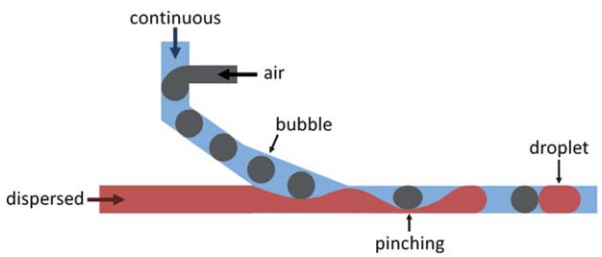

Fig. 1 Schematic of bubble-triggered drop maker. The device consists of three junctions: a jetting junction into which the dispersed phase is injected, a bubbling junction into which the air and continuous phases are injected and the bubbles formed, and the triggering junction, where the jet and bubbles are forced together, and drops are formed. If the bubbles were not present, the jet would be stable due to the very high flow rates, exiting the device without breaking into drops. However, the air bubbles deform the jet, creating pinched regions that are unstable to the Rayleigh–Plateau instability. When the pinched regions break, the fluid between consecutive bubbles becomes the drops.

School of Engineering and Applied Sciences/Department of Physics, Harvard University, Cambridge, Massachusetts, USA +1 617-495-3275. E-mail: adam.abate@ucsf.edu

† Electronic supplementary information (ESI) available: fast camera videos of air-bubble triggered drop formation. See DOI: 10.1039/c1lc20108e

even at very high flow rates. After the bubbles are formed, they approach the triggering junction where they are forced alongside the jet, as illustrated in Fig. 1. In this example, single emulsions are formed by breaking apart a homogenous jet.

To form double emulsions with this mechanism, we use a cross channel for the jetting junction; this allows two fluids to be injected, for the creation of a coaxial jet. For example, the inner fluid of the double emulsion can be injected into the central inlet, and the middle fluid into the two side inlets. This forms a coaxial jet, consisting of the inner fluid surrounded by the middle fluid. The coaxial jet extends into the triggering junction, where it is deformed by the air bubbles and pinched into double emulsion drops.

To investigate the physics of the coaxial jet pinching, we record movies of the process with a fast camera. The bubble-triggered double emulsion maker is fabricated in poly(dimethylsiloxane) (PDMS) using the techniques of soft lithography (see ESI† for drawings of the device).[24] The device is treated to make it hydrophobic by flushing Aquapel through the channels, and then baking them in an oven set to 65 °C for 20 min. As fluids for the double emulsions, we use octanol for the inner phase, water with sodium dodecyl sulfate at 1 wt% as the middle phase, and HFE-7500 fluorocarbon oil with the ammonium salt of Krytox 157 FSL at 1.8 wt% as the continuous phase.

The octanol and water are injected into the central and side inlets of the cross-channel junction, forming a coaxial jet of octanol within water in the triggering junction, as shown to the far left for $t = 0$ ms in Fig. 2. Air is injected into the inner-phase inlet of the T-junction, and fluorocarbon oil is injected into the continuous phase inlet, forming bubbles that then enter the triggering junction. As the bubbles approach the triggering junction, they are forced alongside the coaxial jet. The channels intersect at an angle in this region, creating sloped walls. This forces the bubbles into jet gradually, minimizing the stresses on the bubbles, so that they are not sheared apart by the high-velocity flow. The jet deforms as the bubbles are forced alongside it, because it has a lower Laplace pressure than the bubbles, as indicated by the arrows for $t = 0.12$ to 0.21 ms in Fig. 2. The forces involved in this process can be estimated from the curvatures of the jets and bubbles. For the curvatures we observe, and the known water–oil and air–oil surface tensions, we calculate a Laplace pressure of 2.6 kPa for the bubbles, compared to only 0.6 Pa for the jet; the bubbles are thus less deformable, allowing them to pinch the jet. As each bubble is wedged into the channel, fluid is expelled from the portion of the jet beside it, as shown for $t = 0.12$ to 0.21 ms in Fig. 2; this creates a pinched region in the jet consisting of a narrow bridge of liquid connecting two bulges on either side, as shown for $t = 0.21$ and 0.24 ms.

The pinched geometry is unstable, because the uneven curvature of the interface generates a pressure differential in the jet that pumps fluid out of the connecting bridge; as the fluid drains, the bridge gets smaller, and is unstable to the Rayleigh–Plateau instability, eventually causing it to break. The time required for this to happen is an important parameter in this drop formation mechanism, because it determines how long the geometry must be maintained for the pinch off to complete; this, in turn, limits the maximum rate of drop formation.

To estimate this pinch time, we calculate the time required for the bridge to drain. The uneven curvature of the interface creates a pressure differential in jet that pumps the fluid out of the connecting bridge. We measure the water–oil surface tension to be ~4 mN m^{-1} with our surfactant. Based in the curvatures of the water–oil interface at the pinch and bulges on either side, we estimate a pumping pressure of 1.4 kPa. This pumping is resisted by the viscous drag of the fluid within the bridge. For Hagen–Poiseuille flow, and modelling the bridge as a cylinder with radius of 2 μm and a length of 6 μm, we calculate a hydrodynamic resistance of 2 kg mm^{-4} ms . For the given pumping pressure, this produces a drainage rate of fluid out of the bridge of 1 pL ms^{-1}. The bridge has a total volume of 0.1 pL, so that we estimate an approximate pinch time of 0.1 ms. This is consistent with the pinch time we observe in movies of the process taken with a fast camera, as shown in $t = 0.24$ to 0.30 ms in Fig. 2.

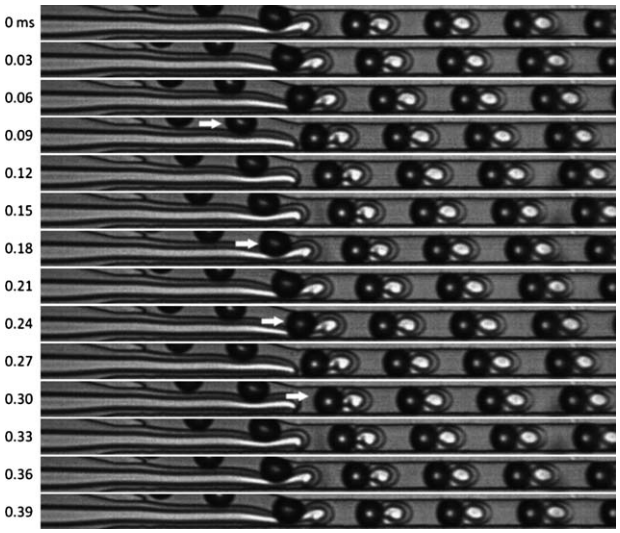

Fig. 2 Formation of monodisperse double emulsions using bubble-triggered drop formation, as visualized with a fast camera. To form double emulsions, a coaxial jet is broken into drops. The coaxial jet is formed by injecting octanol and water into a cross-junction just upstream of the pictured triggering junction. By injecting the octanol into the central channel of the cross-junction and water into the side channels, a coaxial jet of octanol surrounded by water is formed; the coaxial jet appears as a bright jet of octanol surrounded by a darker sheath of water. The bubbles are formed in a T-junction also upstream, and deform the jet when forced alongside it in the triggering junction; the bubbles appear as the very dark circles with a bright spot in the centre. The octanol, water, and fluorocarbon oil are injected at flow rates of 50, 100, and 400 μL h^{-1}, respectively, and the air at a pressure of ~140 kPa. The drop formation frequency is 6.0 kHz. The channel is 25 μm in width, with a square cross section. The arrows follow a single bubble as it pinches off a double emulsion droplet.

For the breakup to complete, the pinched geometry must be maintained longer than the pinch time; otherwise, the jet will exit the channel without breaking into drops. This time thus limits the maximum rate of drop formation. For the flow velocities investigated here, the bubble travels alongside the jet only 32 μm over this time; breakup thus occurs almost instantaneously compared to the rest of the flow dynamics. If the velocities were increased sufficiently, however, the bubble could exit the channel before pinch off completed.

Like other drop formation mechanisms, bubble-triggered drop formation can produce monodisperse drops, though it does so at much faster rates. With bubble-triggered drop formation, it is also possible to control drop size, because this parameter depends on the

volume of fluid partitioned between consecutive bubbles. To characterize the ability to control drop size, we vary the bubble spacing and measure the corresponding drop sizes. When no bubbles are present, the jet is entirely stable, exiting the device as a continuous, unbroken stream of fluid, as shown for $F = 0$ kHz in Fig. 3. As we increase the air pressure we begin to form bubbles at a low frequency; this results in a large spacing between bubbles, and long jet plugs, as shown for $F = 1.9$ kHz in Fig. 3; after pinch off, these plugs pull themselves into large drops. As the air pressure is increased, the bubbles are formed more rapidly; the plugs between consecutive bubbles become shorter, resulting in smaller drops, $F = 2.8$ to 6.0 kHz, Fig. 3. If the air pressure is increased further, the bubbles enter even more rapidly; at this point, however, the spacing is no longer uniform, and the resulting drops are polydisperse, as shown for $F =$ 7.4 kHz Fig. 3.

This change in behaviour at high bubble frequency can be understood by considering the Laplace pressure at the tip of the liquid jet. If the bubbles are introduced too rapidly, there is little time for the tip to extend into the triggering channel before being squeezed by the bubble; consequently, the tip is small and has a large Laplace pressure. This makes the tip harder to deform and, in some instances, may cause the bubble to slide over the tip without pinching off a drop. When the next bubble is injected, a slightly larger drop will be produced, because it will be composed of the fluid collected over the two bubble cycles. This can lead to alternating sequences of small and large drops, or polydisperse drops, as shown for $F = 7.4$ kHz in Fig. 3. It limits the smallest size that the drops can be formed:

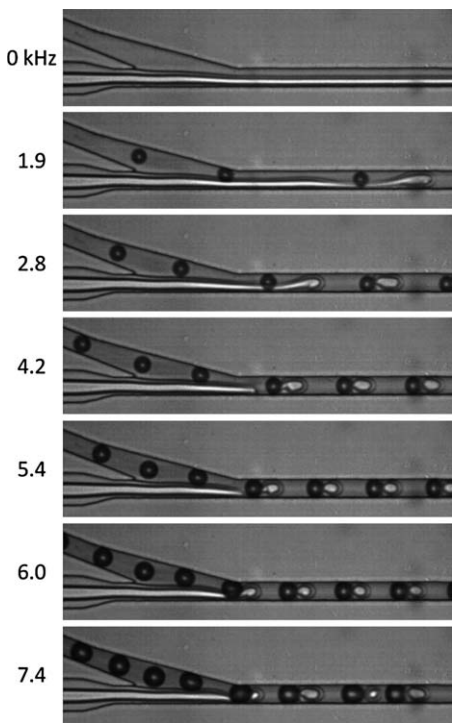

Fig. 3 The size of the drops formed depends on the bubble injection frequency: slower bubble injection results in a long spacing between bubbles, and correspondingly larger drops, while a faster injection frequency results in a shorter spacing, and smaller drops. The octanol, water, and fluorocarbon oil are injected at flow rates of 50, 100, and 400 μL h^{-1}, respectively, and the air pressure is varied between 120 and 145 kPa. The channel is 25 μm in width, with a square cross section.

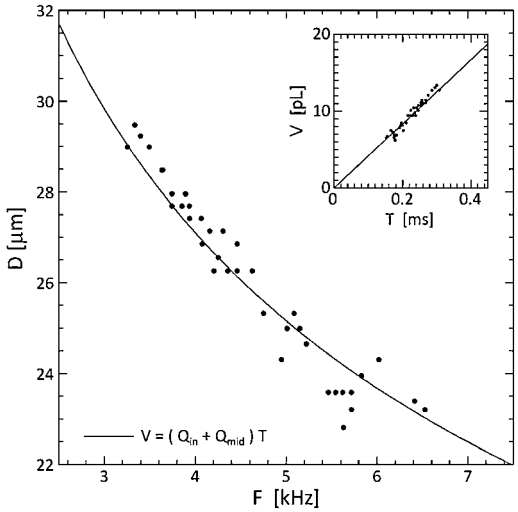

Fig. 4 Drop diameter as a function of triggering frequency and, inset, drop volume as a function of trigger period. In bubble-triggered drop formation, the size of the drops formed depends on the bubble spacing, which can be controlled by adjusting the bubble frequency and the flow velocities of the inner and middle phases. The solid curves in both plots correspond to the scaling predicted by triggered drop formation.

Typically, drops no smaller than the triggering channel can be formed.

Drop size can thus be controlled by adjusting bubble spacing, which can, in turn, be controlled with two parameters. For fixed jet flow rate, reducing bubble frequency increases bubble spacing, leading to larger drops. Similarly, for fixed bubble frequency, increasing jet flow rate increases bubble spacing, also leading to larger drops. Drop volume thus depends on the product of the dispersed phase flow rate and bubble period, $V = (Q_{in} + Q_{mid})T$. To investigate whether this scaling is correct, we plot the drop diameter as a function of the bubble frequency in Fig. 4; we also plot the bubble volume as a function of the period inset in the figure, for easier comparison with the functional form. In both plots, the drop size scaling agrees with this functional form, demonstrating that with bubble-triggered drop formation, drop size can be controlled.

Conclusions

Bubble-triggered drop formation allows monodisperse drops to be formed with controlled size, even under jetting flow conditions. This allows production of monodisperse emulsions at rates much faster than conventional mechanisms, including T-junction and flow-focus mechanisms. Another advantage of this approach is that it requires a minimal amount of continuous phase to form the drops, because a majority of the volume in the continuous phase is occupied by the bubbles, making this a cost-effective drop formation strategy as well. One complication, however, is that in addition to drops, the resultant emulsion contains air bubbles, which may need to be removed from the emulsion, depending on the application. For example, if additional operations must be performed on the drops, such as injecting them with reagents or splitting them, the bubbles may get in the way. In these cases, they should be removed inline using passive hydrodynamic sorting;[25,26] this removes the bubbles by exploiting their different flow characteristics compared to the drops, for example,

based on differences in their size and viscosity. If the bubbles do not need to be removed inline, the emulsion could be collected and the bubbles allowed to float to the surface, where they could be easily skimmed away. The speed and simplicity of this method should make it useful for applications that require extremely high-throughput drop formation. This, coupled with the ability to create multiple emulsions, should make it attractive for large-scale synthesis of polymer spheres and core-shell capsules.

We thank Christian Holtze for helpful discussions. This work was supported by the NSF (DMR-1006546), the Harvard MRSEC (DMR-0820484), and the Massachusetts Life Sciences Center.

Notes and references

1 P. B. Umbanhowar, V. Prasad and D. A. Weitz, *Langmuir*, 2000, **16** (2), 347–351.
2 A. S. Utada, E. Lorenceau, D. R. Link, P. D. Kaplan, H. A. Stone and D. A. Weitz, *Science*, 2005, **308**(5721), 537–541.
3 L. Y. Chu, A. S. Utada, R. K. Shah, J. W. Kim and D. A. Weitz, *Angew. Chem., Int. Ed.*, 2007, **46**(47), 8970–8974.
4 R. K. Shah, H. C. Shum, A. C. Rowat, D. Lee, J. J. Agresti, A. S. Utada, L. Y. Chu, J. W. Kim, A. Fernandez-Nieves, C. J. Martinez and D. A. Weitz, *Mater. Today*, 2008, **11**(4), 18–27.
5 A. R. Abate and D. A. Weitz, *Small*, 2009, **5**(18), 2030–2032.
6 D. Dendukuri, K. Tsoi, T. A. Hatton and P. S. Doyle, *Langmuir*, 2005, **21**(6), 2113–2116.
7 S. Q. Xu, Z. H. Nie, M. Seo, P. Lewis, E. Kumacheva, H. A. Stone, P. Garstecki, D. B. Weibel, I. Gitlin and G. M. Whitesides, *Angew. Chem., Int. Ed.*, 2005, **44**(5), 724–728.
8 T. Nisisako, T. Torii, T. Takahashi and Y. Takizawa, *Adv. Mater.*, 2006, **18**(9), 1152.
9 R. F. Shepherd, J. C. Conrad, S. K. Rhodes, D. R. Link, M. Marquez, D. A. Weitz and J. A. Lewis, *Langmuir*, 2006, **22**(21), 8618–8622.
10 C. H. Chen, R. K. Shah, A. R. Abate and D. A. Weitz, *Langmuir*, 2009, **25**(8), 4320–4323.
11 B. T. Kelly, J. C. Baret, V. Taly and A. D. Griffiths, *Chem. Commun.*, 2007, 1773–1788.
12 J. Clausell-Tormos, D. Lieber, J. C. Baret, A. El-Harrak, O. J. Miller, L. Frenz, J. Blouwolff, K. J. Humphry, S. Koster, H. Duan, C. Holtze, D. A. Weitz, A. D. Griffiths and C. A. Merten, *Chem. Biol.*, 2008, **15**(8), 875–875.
13 D. T. Chiu and R. M. Lorenz, *Acc. Chem. Res.*, 2009, **42**(5), 649–658.
14 J. J. Agresti, E. Antipov, A. R. Abate, K. Ahn, A. C. Rowat, J. C. Baret, M. Marquez, A. M. Klibanov, A. D. Griffiths and D. A. Weitz, *Proc. Natl. Acad. Sci. U. S. A.*, 2010, **107**(9), 4004–4009.
15 L. Granieri, J. C. Baret, A. D. Griffiths and C. A. Merten, *Chem. Biol.*, 2010, **17**(3), 229–235.
16 S. L. Anna, N. Bontoux and H. A. Stone, *Appl. Phys. Lett.*, 2003, **82** (3), 364–366.
17 P. Guillot and A. Colin, *Phys. Rev. E: Stat., Nonlinear, Soft Matter Phys.*, 2005, **72**(6), 066301.
18 P. Garstecki, M. J. Fuerstman, H. A. Stone and G. M. Whitesides, *Lab Chip*, 2006, **6**(5), 693–693.
19 A. S. Utada, A. Fernandez-Nieves, H. A. Stone and D. A. Weitz, *Phys. Rev. Lett.*, 2007, **99**(9), 094502.
20 T. Cubaud and T. G. Mason, *Phys. Fluids*, 2008, **20**(5), 053302–053311.
21 A. S. Utada, A. Fernandez-Nieves, J. M. Gordillo and D. A. Weitz, *Phys. Rev. Lett.*, 2008, **100**(1), 014502.
22 P. Guillot, A. Colin, A. S. Utada and A. Ajdari, *Phys. Rev. Lett.*, 2007, **99**(10), 104502.
23 K. J. Humphry, A. Ajdari, A. Fernandez-Nieves, H. A. Stone and D. A. Weitz, *Phys. Rev. E: Stat., Nonlinear, Soft Matter Phys.*, 2009, **79**(5), 056310.
24 Y. Xia and G. M. Whitesides, *Angew. Chem., Int. Ed.*, 1998, **37**(5), 550–575.
25 M. Chabert and J. L. Viovy, *Proc. Natl. Acad. Sci. U. S. A.*, 2008, **105** (9), 3191–3196.
26 H. Maenaka, M. Yamada, M. Yasuda and M. Seki, *Langmuir*, 2008, **24**(8), 4405–4410.

